

Rediscover Climate Change during Global Warming Slowdown via Wasserstein Stability Analysis

Zhiang Xie¹, Dongwei Chen², and Puxi Li³

¹Department of Earth and Space Sciences, Southern University of Science and Technology, Shenzhen
518055, Guangdong, China

²School of Mathematical and Statistical Sciences, Clemson University, Clemson 29641, SC, USA

³State Key Laboratory of Severe Weather, Chinese Academy of Meteorological Sciences, China
Meteorological Administration, Beijing 100081, China

Key Points:

- We introduce a novel method called Wasserstein Stability Analysis (WSA) to detect changes in Probability Distribution Function (PDF)s.
- WSA can detect signals related to La-Nina-like extreme event shifts in the eastern Pacific during global warming hiatus.
- During the hiatus in global warming, the WSA is able to detect a change in the temperature constraint value caused by the disappearance of sea ice.

arXiv:2303.18067v1 [physics.ao-ph] 29 Mar 2023

Abstract

Climate change is one of the key topics in climate science. However, previous research has predominantly concentrated on changes in mean values, and few research examines changes in Probability Distribution Function (PDF). In this study, a novel method called Wasserstein Stability Analysis (WSA) is developed to identify PDF changes, especially the extreme event shift and non-linear physical value constraint variation in climate change. WSA is applied to 21st-century warming slowdown period and is compared with traditional mean-value trend analysis. The result indicates that despite no significant trend, the central-eastern Pacific experienced a decline in hot extremes and an increase in cold extremes, indicating a La Nina-like temperature shift. Further analysis at two Arctic locations suggests sea ice severely restricts the hot extremes of surface air temperature. This impact is diminishing as sea ice melts. Overall, based on detecting PDF changes, WSA is a useful method for re-discovering climate change.

1 Introduction

How climate system evolves with time is one of the essential topics in climate science. The Intergovernmental Panel on Climate Change Sixth Assessment Report (IPCC AR6) pointed out that the global mean of surface air temperature (SAT) follows a general warming trend since 20th century, which is mainly attributed to the human influence. Consequently, considerable work is devoted to discussing the mean temperature warming trend and its spatial distribution (Delworth & Knutson, 2000; Delworth et al., 2015; Huang et al., 2017; Li et al., 2015).

Mean value is one of the most significant statistical characteristics of climate data, as it represents the overall energy condition and even the low-frequency variability of the climate system. However, the human-induced mean value warming of SAT may be partially countered by internal variability or external forcing. Thus, the warming trend is not always strong and rising at the same pace. As a result, the mean value change, especially the mean value trend, cannot give sufficient information about climate change. During 1998 - 2013 period, global mean surface temperature experienced a slower increase, which is referred to as "global warming hiatus" in some studies (Modak & Mauritsen, 2021; Douville et al., 2015; Kosaka & Xie, 2013; Lee et al., 2015; Delworth et al., 2015; England et al., 2014; Li et al., 2015). However, during this period, a series of climate changes are still recorded, such as extreme events (Johnson et al., 2018) and La-Nina-like Pacific temperature pattern (Kosaka & Xie, 2013). Unfortunately, it is difficult to detect these climate change signals by trend or mean value analysis since the relevant signals during the warming slowdown period are pretty weak. Thus the observational climate change signal during the slowdown period is challenging to detect. This issue is mainly because mean value only uses partial information (first moment) from climate data and does not reflect the whole climate change picture. Naturally, one may ask a further question: how can we detect the climate change signal when the mean value roughly remains constant and there is no significant trend?

A general solution is to track the change in Probability Distribution Function (PDF) that not only includes moments like mean value and variance, but also contains extreme events and critical values. Recently, a new mathematical tool from optimal transport, called Wasserstein distance, sheds more light on this question. Mathematically speaking, Wasserstein distance is induced from Monge-Kantorovich mass transportation problem that studies how to transport mass from a probability measure μ to another probability measure ν in the cheapest way. It provides a powerful metric to quantify the similarities and discrepancies between two distributions (Santambrogio, 2015; Figalli & Glaudo, 2021). Based on Wasserstein distance, we develop a novel method, named as Wasserstein Stability Analysis (WSA), to discover the climate change signals such as extremes and physical value constraints. Compared to mean value analysis, WSA could help researchers directly identify the significant PDF variability, which gives us a better insight into climate change.

The paper is organized as follows. In section 2, we give a description to the data set and WSA algorithm. Optimal mass transportation and Wasserstein distance are also briefly introduced. In section 3, we apply WSA to global warming slowdown period. Through the new method, we obtain a clear equatorial eastern Pacific signal that is highlighted in previous studies and an evident physical value constraint change in the Arctic that is not fully explored. Finally, in section 4, we draw a conclusion and discuss the future work.

2 Data and Method

This section is divided into two parts. In the first section, we give a description of the dataset used in this article. Then we give a brief introduction to Wasserstein distance and the Wasserstein Stability Analysis.

2.1 Dataset

The surface 2 meters air temperature data in this work are obtained from ERA5 dataset ($0.25^\circ \times 0.25^\circ$, single layer, half day time interval) from 1998 to 2013 (Hersbach et al., 2020). And the spatial range is global. To better represent the large-scale signal and accelerate the data processing, we regrid the original data set into daily data with a horizontal resolution of $2.5^\circ \times 2.5^\circ$ by spatial and temporal average.

The sea ice data used in the study come from Hadley Centre Sea Ice and Sea Surface Temperature monthly data set (HadISST), with $1^\circ \times 1^\circ$ horizontal resolution (Rayner et al., 2003). The time range is from 1998 to 2013 and the spatial range is still global.

2.2 Wasserstein Stability Analysis

2.2.1 Introduction to Wasserstein distance

In 1781, Gaspard Monge proposed the concept of optimal transport from one practical situation: if one uses soil to build fortifications, what is the cheapest way to transport the soil? This scenario leads to the following Monge formulation of optimal transport

$$\inf_{T_{\#}\mu=\nu} \int_X c(x, T(x)) d\mu(x), \quad (1)$$

where $\nu = T_{\#}\mu$ means the transport map T pushes forward the probability measure $\mu \in \mathcal{P}(X)$ to another probability measure $\nu \in \mathcal{P}(Y)$ and $c(x, T(x)) = |x - T(x)|$ is the cost of transporting unit mass from x to $T(x)$. In the 1940s, Leonid Kantorovich revisited Monge's problem and gave relaxation to Monge's formulation by splitting the mass. Kantorovich relaxation leads to the following formulation of optimal transport

$$\inf_{\pi \in \Pi(\mu, \nu)} \int_{X \times Y} c(x, y) d\pi(x, y), \quad (2)$$

where $\pi \in \Pi(\mu, \nu) = \{\pi \in \mathcal{P}(X \times Y) : P_{X\#}\pi = \mu, P_{Y\#}\pi = \nu\}$ means π is a joint distribution (transport plan) with marginals μ and ν . The metric side of Kantorovich formulation makes it valid to quantify the similarities between probability measures μ and ν via p-Wasserstein distance, given as below

$$\mathcal{W}_p(\mu, \nu) = \left(\inf_{\pi \in \Pi(\mu, \nu)} \int_{X \times Y} |x - y|^p d\pi(x, y) \right)^{\frac{1}{p}}, \quad (3)$$

Compared to other PDF similarity metric like Kullback–Leibler divergence, Wasserstein distance is rigorously defined and satisfies the metric axioms (Figalli & Glaudo, 2021). Wasserstein distance provides a powerful metric to quantify the similarities and discrepancies between probability distributions, and has been applied to climate science, such as model evaluation (Vissio et al., 2020), oceanographic data analysis (Hyun et al., 2022), and data assimilation (Tamang, 2022). In this work, we will use the earth mover's distance, i.e. $p = 1$.

2.2.2 Wasserstein Stability Analysis

Different from trend and mean value analysis, Wasserstein distance is designed to evaluate the magnitude of PDF change quantitatively. In the null hypothesis, we usually assume that the PDF of one variable is stable and follows the same distribution. In that sense, we claim that the variable has an unstable PDF if the Wasserstein distance (W-distance) between its current state and a reference state is out of some confidence interval, representing a significant change from one climate stage to another. Therefore, the significant PDF change signal is detected, and the climate change details can be further explored. Hence, in this part, we develop a novel algorithm (Algorithm 1) named as WSA to detect unstable PDF change signals.

The new method is mainly divided into two steps: W-distance test and PDF analysis. The details are as follows:

(1). *W-distance test.* Given two samples X and Y with the same length, both series are first normalized individually by the following scalar

$$\frac{x - \mu}{\sigma} \quad (4)$$

where μ is the mean value and σ is the standard deviation. Then Wasserstein distance $\mathcal{W}_1(X, Y)$ between X and Y are obtained after normalization. It is worth to note that this normalization is necessary since the geographic difference may lead to a large variation in W-distance. For example, the high surface temperature variation at high latitudes usually leads to a larger W-distance than its counterpart in tropical zones. Nevertheless, it does not necessarily mean the PDF change at high latitudes is stronger than that at low latitudes.

Our significance test is based on the Monte Carlo test (Xie et al., 2017). The null hypothesis H_0 of WSA is that the PDF discrepancy between X and Y can be explained by the white noise. Clearly, the alternate hypothesis (H_1) is that the discrepancy of PDFs between X and Y results from factors other than white noise. We generate two new samples, X_N and Y_N , by adding white noise to X and Y . Then one could obtain the W-distance $\mathcal{W}_1(X_N, Y_N)$ between X_N and Y_N . White noise addition is performed 500 times. Therefore, one could get a confidence interval (C.I.) of W-distances. Under the null hypothesis H_0 that the distribution discrepancy between X and Y can be explained by the white noise, $\mathcal{W}_1(X, Y)$ must be indistinguishable from $\mathcal{W}_1(X_N, Y_N)$. Given confidence level α , one would expect that $\mathcal{W}_1(X, Y)$ is within the confidence interval of $\{\mathcal{W}_1(X_N, Y_N)\}_{N=1}^{500}$. If not, H_0 is rejected, and one could claim that the distribution discrepancy between X and Y is not from white noise with the confidence level of $1 - \alpha$.

In this study, a higher confidence level of $\alpha = 99\%$, rather than the common 95%, is used, since W-distance is very sensitive to the PDF change. Since we used a large size of samples, according to the central limit theorem, the amplitude of white noise is set as one standard deviation of given samples individually.

(2). *PDF analysis.* After detecting the significant PDF change zone, we plot two PDFs and the corresponding change to understand why W-distance is significant. The next section will use two examples to demonstrate how it functions.

3 Results

We start the method evaluation by comparing WSA and linear trend analysis of mean values (Figure 1). Figure 1a depicts the Wasserstein distance between SAT PDFs during 1998-2005 and 2006-2013. The central eastern Pacific has the greatest W-distance, with values ranging from 0.08 to 0.24; nevertheless, there is no discernible trend (Figure 1b). Another noticeable W-distance signal could be seen over the Barents-Kara Sea, which is located inside a significant warming trend zone in the Arctic (Figure 1b). Although there are some other dispersed significant W-distance regions over the Indian Ocean and South

America, the following analysis will mainly focus on signals over central eastern Pacific and Barents-Kara Sea to highlight the information that W-distance can provide about climate change. In order to achieve this, we selected three special sites to do further PDF analysis:

1. Site A (90 °W, 0): one site with a significant W-distance signal but without a significant linear trend;
2. Sites B (66 °E,79 °N) and C (131 °E,79 °N): both sites exhibit significant linear trends. However, Site B has a significant W-distance while C does not.

Figure 2 shows the SAT PDFs and their changes from the 1998-2005 period to the 2006-2013 period at Site A. The mean value and standard deviation stay relatively stable within the 1998-2005 and 2006-2013 periods. However, in the second period, the hot extremes (more than two standard deviations, 25 °C) decrease by more than ten days per year, while the mild hot events (near one standard deviation) increase by roughly 30 days per year. Meanwhile, the cold extremes (less than -2 standard deviations, 19 °C) increase by more than ten days per year, while the mild cold events (near -1 standard deviation) decrease by more than 30 days per year. The hot extreme decreasing and cold extreme increasing indicate a La Nina-like SAT shift. Many recent studies argue that the 21st slowdown period is in the negative phase of Pacific Decadal Oscillation, and this strong low-frequency variability canceled out some parts of the global warming trend (Douville et al., 2015; Kosaka & Xie, 2013; Lee et al., 2015; England et al., 2014). Our W-distance result agrees well with this conclusion and extends the results from the perspective of PDF change. Indeed, even though the mean value does not show a significant trend, we can still observe the La Nina-like SAT shift from extreme event change, which is reflected by the strong PDF change and the corresponding significant W-distance.

Site B is another region with a significant W-distance, suggesting a strong PDF change from the 1998-2005 period to the 2006-2013 period (Figure 3 (a) and (c)). At Site B, SAT shows significant warming from -10.2 °C to -6.4 °C. Meanwhile, the standard deviation decreases from 9.9 °C to 7.4 °C, indicating an elimination of SAT variation. Since Site B is located within a zone covered by sea ice, the maximum SAT is strongly constrained to being near the frozen line in both periods, and thus this causes a sharp frequency jump near the frozen line (Figure 3 (a)). However, as the mean value increases and the standard deviation decreases during the second period, the frozen line at Site B shifts significantly to the left. As a result, the frequency peak of hot events shifts to the left. Meanwhile, the slope near the frozen line becomes flatter, leading to a smoother PDF shape. In contrast, Site C exhibits a change that follows a similar pattern but is considerably smaller in extent in terms of mean value, standard deviation, and frozen line shift (Figure 3 (b) and (d)). Consequently, W-distance at Site C is smaller than that at Site B and fails the 99% significant test. Actually, the existence of sea ice strongly limits the maximum surface temperature and the corresponding surface air temperature near the frozen line. Therefore, the sharp peak shape of SAT PDF appears in regions covered by sea ice. Nevertheless, regions with normal ocean conditions are expected to have a more uniform distribution. Therefore, the alteration in Site B and Site C suggests that the variability in sea ice concentration may play a role in the SAT PDF change from the first to the second period.

By checking the full-time series in two periods, we can better understand the PDF change at Site B and Site C. From 1998-2005 period to 2006-2013 period, the interval with ± 1 standard deviation shrinks and moves upward at Site B because of the change in mean value and standard deviation (Figure 4(a)). Clearly, this change leads to most of the SAT variabilities being below +1 standard deviation and also more cold extremes. For Site C, we can see a similar change but in a much smaller magnitude (Figure 4 (b)). As discussed, this difference can be attributed to the sea ice and its strong temperature constraint. Figure 4 (c) shows the sea ice concentration change between 1998-2005 and 2006-2013. We can see that Site B is in a zone where sea ice is melting the most. Hence the PDF change at Site B is the most intense. As a comparison, Site C also experiences a sea ice loss but to a relatively small extent. As the temperature increases, the sea ice concentration decreases, and the

effect of sea ice restriction gradually fades. This is why Site C also displays a similar PDF change but with a less significant level. In summary, the significant W-distance change at Site B implies the removal of physical temperature constraint imposed by sea ice that causes the sharp peak near the frozen line in PDF.

4 Conclusion and Discussion

In this work, we develop a novel method called WSA to detect climate change signals. The results indicate that WSA shows some advantages compared with the classic mean value analysis in certain cases. The classic trend analysis based on mean value cannot detect the extreme event signals in the central eastern Pacific Ocean during warming hiatus, while WSA can easily identify the La Nina-like temperature PDF shift. Additionally, due to the strong temperature constraint of sea ice, the sea ice cover area shows a different PDF pattern compared to the open ocean. As a result, unlike mean value analysis detecting significant trend regions, WSA can find out the strong sea-ice-loss area during warming hiatus, indicating a fundamental physical property change of the surface.

It should be noted that the discussion of PDF change during the global warming slow-down period is incomplete in this study. We just chose several typical sites to illustrate the abundant information from the significant PDF change and verify the capability of the WSA algorithm. A more detailed discussion on scattered significant signals in the Indian Ocean and South America is another interesting topic. Meanwhile, we only applied the WSA in SAT in this study. Similarly, we can also apply the WSA to precipitation, wind speed, and pressure, which may also offer more insights into climate change.

However, the current WSA method could only detect whether the distribution has changed or not, and the direction of change is not well depicted. For example, Fig. 1(a) can only provide us a clue to discover PDF change signals, but cannot directly tell us whether most of the regions have more cold extremes or warm extremes. Therefore, how to measure the direction of PDF change is still a challenging topic and needs to be further explored in the future.

Data Availability Statement

The surface 2 meters air temperature data is from ERA5 reanalysis products of the European Centre for Medium-Range Weather Forecast (ECMWF) (Hersbach et al., 2020), which could be accessed online via <https://www.ecmwf.int/en/forecasts/dataset/ecmwf-reanalysis-v5>. The sea ice data is from the Hadley Centre Sea Ice and Sea Surface Temperature data set (HadISST) of Met Office in British (Rayner et al., 2003), which could be accessed online via <http://www.metoffice.gov.uk/hadobs/hadisst/>.

Software Availability Statement

The code of Wasserstein Stability Analysis can be found at <https://github.com/YMI33/wasserstein>.

Acknowledgement

The authors greatly appreciate the comments of Dr. Zhaolu Hou from the Ocean University of China and Dr. Shuailei Yao from the Institute of Atmospheric Physics, Chinese Academy of Sciences. This work is supported by the National Natural Science Foundation of China 42005039.

References

- Delworth, T. L., & Knutson, T. R. (2000). Simulation of early 20th century global warming. *Science*, 287(5461), 2246–2250. doi: 10.1126/science.287.5461.2246
- Delworth, T. L., Zeng, F., Rosati, A., Vecchi, G. A., & Wittenberg, A. T. (2015). A link between the hiatus in global warming and North American drought. *Journal of Climate*, 28(9), 3834–3845. doi: 10.1175/JCLI-D-14-00616.1
- Douville, H., Voldoire, A., & Geoffroy, O. (2015). The recent global warming hiatus: What is the role of Pacific variability? *Geophysical Research Letters*, 42(3), 880–888. doi: 10.1002/2014GL062775
- England, M. H., McGregor, S., Spence, P., Meehl, G. A., Timmermann, A., Cai, W., ... Santoso, A. (2014). Recent intensification of wind-driven circulation in the Pacific and the ongoing warming hiatus. *Nature Climate Change*, 4(3), 222–227. doi: 10.1038/nclimate2106
- Figalli, A., & Glaudo, F. (2021). *An invitation to optimal transport, wasserstein distances, and gradient flows* (Vol. 23). EMS PRESS.
- Hersbach, H., Bell, B., Berrisford, P., Hirahara, S., Horányi, A., Muñoz-Sabater, J., ... others (2020). The era5 global reanalysis. *Quarterly Journal of the Royal Meteorological Society*, 146(730), 1999–2049.
- Huang, J., Zhang, X., Zhang, Q., Lin, Y., Hao, M., Luo, Y., ... Zhang, J. (2017). Recently amplified arctic warming has contributed to a continual global warming trend. *Nature Climate Change*, 7(12), 875–879. Retrieved from <http://dx.doi.org/10.1038/s41558-017-0009-5> doi: 10.1038/s41558-017-0009-5
- Hyun, S., Mishra, A., Follett, C. L., Jonsson, B., Kulk, G., Forget, G., ... others (2022). Ocean mover’s distance: using optimal transport for analysing oceanographic data. *Proceedings of the Royal Society A*, 478(2262), 20210875.
- Johnson, N. C., Xie, S. P., Kosaka, Y., & Li, X. (2018). Increasing occurrence of cold and warm extremes during the recent global warming slowdown. *Nature Communications*, 9(1), 4–6. Retrieved from <http://dx.doi.org/10.1038/s41467-018-04040-y> doi: 10.1038/s41467-018-04040-y
- Kosaka, Y., & Xie, S. P. (2013). Recent global-warming hiatus tied to equatorial Pacific surface cooling. *Nature*, 501(7467), 403–407. Retrieved from <http://dx.doi.org/10.1038/nature12534> doi: 10.1038/nature12534
- Lee, S. K., Park, W., Baringer, M. O., Gordon, A. L., Huber, B., & Liu, Y. (2015). Pacific origin of the abrupt increase in Indian Ocean heat content during the warming hiatus. *Nature Geoscience*, 8(6), 445–449. doi: 10.1038/NGEO2438
- Li, Q., Yang, S., Xu, W., Wang, X. L., Jones, P., Parker, D., ... Gao, Y. (2015). China experiencing the recent warming hiatus. *Geophysical Research Letters*, 42(3), 889–898. doi: 10.1002/2014GL062773
- Modak, A., & Mauritsen, T. (2021). The 2000–2012 Global Warming Hiatus More Likely With a Low Climate Sensitivity. *Geophysical Research Letters*, 48(9), 1–9. doi: 10.1029/2020GL091779
- Rayner, N. A., Parker, D. E., Horton, E. B., Folland, C. K., Alexander, L. V., Rowell, D. P., ... Kaplan, A. (2003). Global analyses of sea surface temperature, sea ice, and night marine air temperature since the late nineteenth century. *Journal of Geophysical Research: Atmospheres*, 108(14). doi: 10.1029/2002jd002670
- Santambrogio, F. (2015). *Optimal transport for applied mathematicians: Calculus of variations, pdes, and modeling* (Vol. 87). Birkhäuser.
- Tamang, S. (2022). *Advancing the predictability of the earth system processes: Insights from optimal mass transport theory* (Doctoral dissertation, University of Minnesota). Retrieved from <https://hdl.handle.net/11299/227930>
- Vissio, G., Lembo, V., Lucarini, V., & Ghil, M. (2020). Evaluating the performance of climate models based on wasserstein distance. *Geophysical Research Letters*, 47(21), e2020GL089385.
- Xie, Z., Duan, A., & Tian, Q. (2017). Weighted composite analysis and its application: an example using ENSO and geopotential height. *Atmospheric Science Letters*, 18(11),

435–440. doi: 10.1002/asl.786

Algorithm 1 Wasserstein Stability Analysis (WSA)

```

1: procedure ( $H_0$ : the discrepancy in distributions between  $X$  and  $Y$  is from white noise,
   with confidence level  $\alpha = 0.01$ )
2:    $X$  and  $Y$  are normalized individually by the  $\frac{x-\mu}{\sigma}$  scalar.
3:   Get  $\mathcal{W}_1(X, Y)$ 
4:    $N \leftarrow 1$ 
5:   while  $N \leq 500$  do
6:      $X_N \leftarrow X + \text{random}(0, 1)$  ▷ add white noise  $N(0, 1)$  to  $X$  and  $Y$ 
7:      $Y_N \leftarrow Y + \text{random}(0, 1)$ 
8:     Get  $\mathcal{W}_1(X_N, Y_N)$  ▷  $X_N$  and  $Y_N$  are series with white noise
9:      $N \leftarrow N + 1$ 
10:  end while
11:  if  $\mathcal{W}_1(X, Y)$  is out of 99% C.I. of  $\{\mathcal{W}_1(X_N, Y_N)\}_{N=1}^{500}$  then
12:    reject  $H_0$  ▷ The discrepancy is not from  $N(0, 1)$ 
13:  else
14:     $H_0$  is not rejected
15:  end if
16: end procedure

```

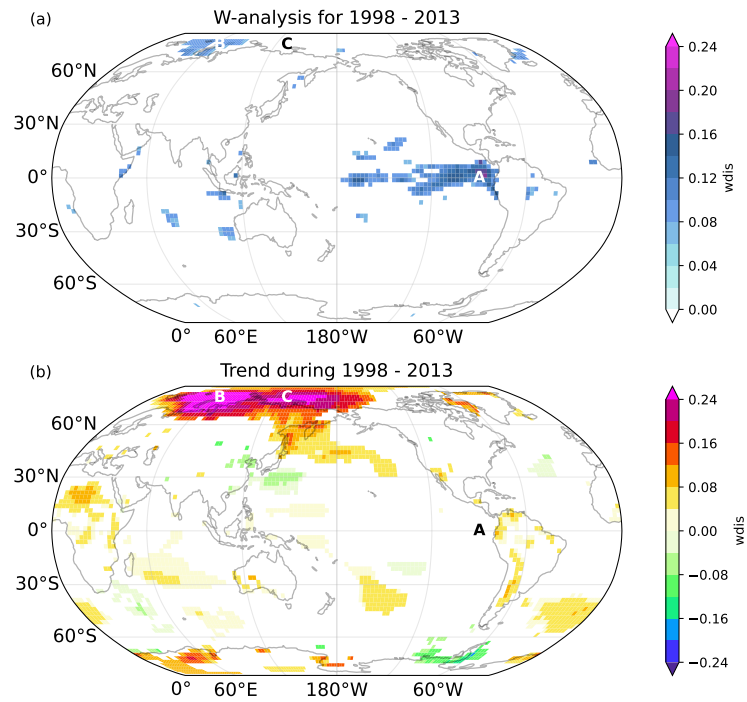


Figure 1. (a) Wasserstein distance between probability distribution functions during 1998-2005 and 2006-2013. (b) Linear trend during 1998-2013. Only statistically significant regions (99% for Wasserstein distance and 95% for linear trend) are shown. Three sites, A (90°W , 0°), B (66°E , 79°N), and C (131°E , 79°N), have been chosen for further analysis.

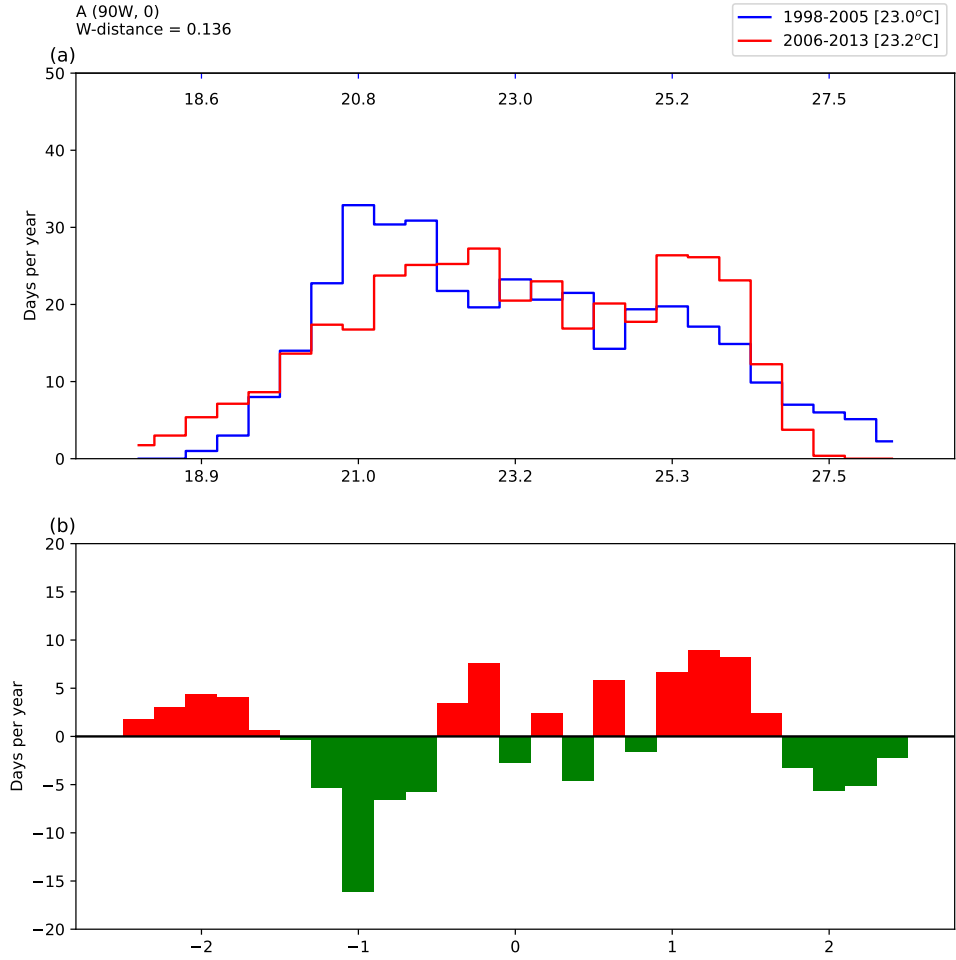


Figure 2. (a) Probability distribution functions (PDFs) for the periods 1998–2005 (blue) and 2006–2013 (red). The bottom tick labels represent observed temperature values from 2006 to 2013, whereas the top tick labels represent observed temperature values from 1998 to 2005. (b) The difference between two PDFs of normalized temperature series at site A (90°W , 0). The frequency has been normalized as days per year. The mean value for the time period is shown by the blanketed number in the legend.

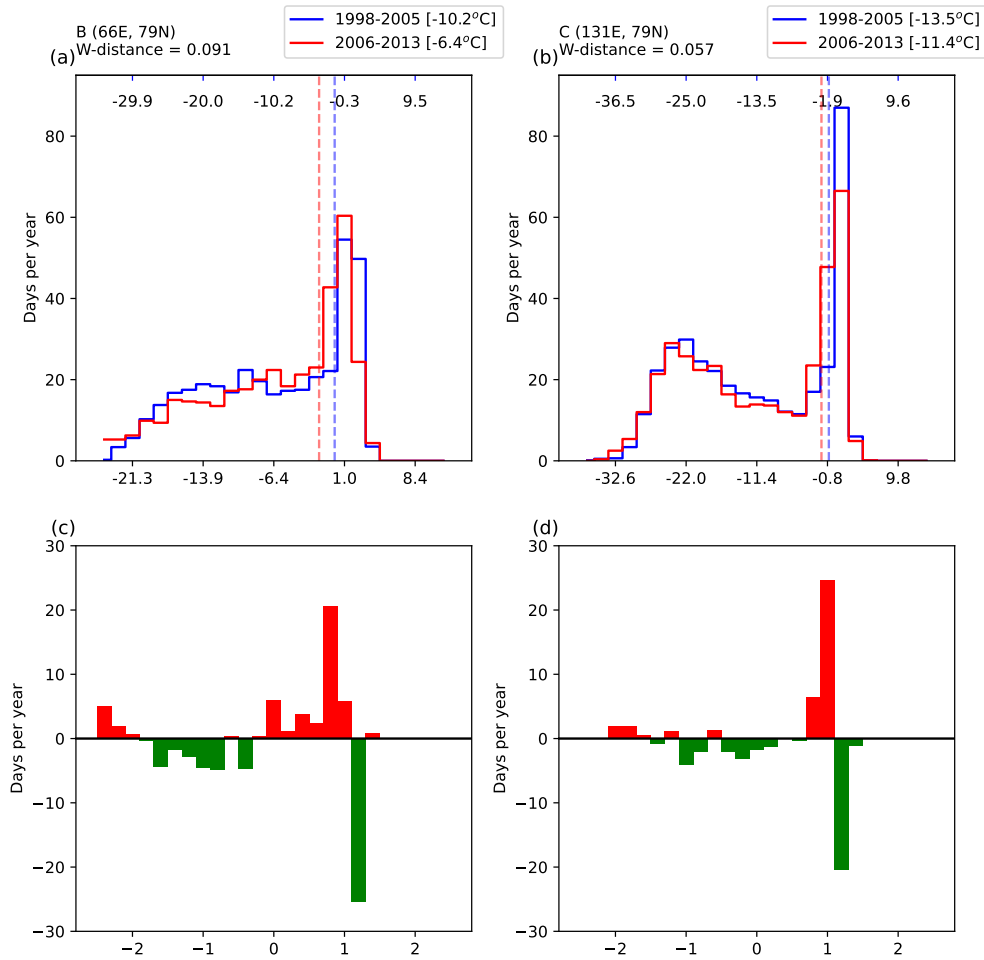


Figure 3. Same as Figure 2. Panel (a) and (c) is for Site B, and Panel (b) and (d) is for Site C. The dashed lines in Panel (a) and (b) represent the ocean frozen temperature (-1.7°C) in two distributions (blue for 1998-2005 and red for 2006-2013).

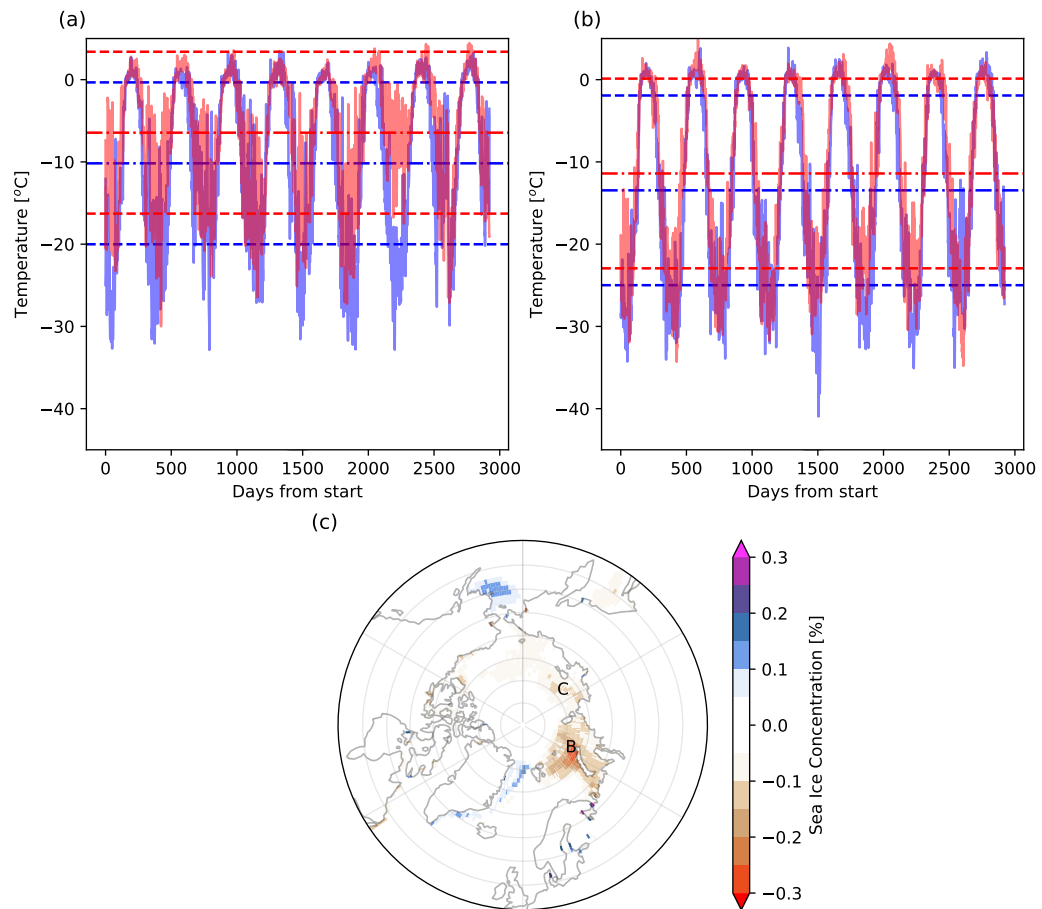


Figure 4. Full daily 2m temperature time series of 1998-2005 (blue) and 2006-2013 (red) at Site B is plotted in Panel (a), and the counterpart at Site C is plotted in Panel (b). Panel (c) shows the sea ice concentration change (unit: %) between 1998-2005 and 2006-2013.